This is a preprint, the final version is subject to change, of the American Mineralogist (MSA)
Cite as Authors (Year) Title. American Mineralogist, in press.
(DOI will not work until issue is live.) DOI: http://dx.doi.org/10.2138/am-2015-4907

The magma plumbing system of the Emeishan large igneous province and its role in basaltic magma differentiation in a continental setting

Yan Tao [a,*], Keith Putirka [b], Rui-Zhong Hu [a], and Chusi Li [c]

[a] State Key Laboratory of Ore Deposit Geochemistry, Institute of Geochemistry, Chinese Academy of Sciences, Guiyang, 550002, China

[b] California State University, Fresno, Department of Earth and Environmental Sciences, 2576 E. San Ramon Ave., MS/ST25, Fresno, CA 93740, USA

[c] Department of Geological Sciences, Indiana University, Bloomington, IN 47405, USA

Revision for American Mineralogist

March 31, 2015

*Corresponding author: Yan Tao

E-mail: taoyan@vip.gyig.ac.cn

Abstract

Magmatic activity of the Emeishan large igneous province (ELIP) of SW China is one of the most significant geological events of the late Paleozoic. The large volume flood basalts plus rare picrites were erupted in Late Permian. Previous studies indicate that the basalts are the derivatives of primary mantle-derived magma by fractional crystallization,

but the depths at which this process took place remain unknown. To answer this question, we use phenocryst compositions and mineral-liquid thermobarometers to determine the P-T conditions of the magma reservoirs where crystallization occurred, then use these data to reconstruct the magma plumbing system of the igneous province. Thermobarometric calculations show that most picrite-hosted clinopyroxene phenocrysts crystallized at ~25 km and 1200 – 1300°C, whereas most basalt-hosted clinopyroxene phenocrysts crystallized at depths < 20 km and temperatures <1200°C. Some picrites containing primitive olivine with Fo up to Fo92 likely formed by eruption of the most primitive magma with composition similar to the primary magma from the deepest reservoir possibly at the Moho. Parental magmas yield mantle potential temperatures of 1740-1810^{o}C, which are the highest such temperatures yet recorded for terrestrial magmas of any age. Less primitive picrites containing both olivine and clinopyroxene phenocrysts formed by eruption of moderately fractionated magma from a reservoir in the middle crust. Basalts and basaltic andesites formed by eruption of the most fractionated magmas from the reservoirs in the upper crust, coinciding with the depths of coeval sulfide ore-bearing and Fe-Ti-V oxide ore-bearing mafic-ultramafic intrusions. The reason that the Emeishan volcanic sequence is dominated by basalts is because most of the mantle-derived magma was trapped in the middle and upper crusts, undergoing variable degrees of crystal fractionation plus crustal contamination before eruption. Primitive picrites are rare because their eruption requires a trans-lithosphere conduit which is difficult to create and maintain due to increasing lithospheric pressure with depth. The results from this study reveal that magma reservoirs at the crustal levels play a critical role in magma differentiation in a continental setting.

Key Words: Magma plumbing system; Flood basalt province; Clinopyroxene phenocrysts; Thermobarometer; Magma differentiation; Emeishan.

Introduction

Magmatism of the Emeishan large igneous province (ELIP) is one of the most significant geological events in the late Paleozoic (Chung and Jahn 1995; Courtillot et al. 1999). The province includes the large volume of continental flood basalts, rare picrites and associated mafic-ultramafic intrusions, which were erupted and emplaced in the Late Permian (Xu et al. 2001; Zhou et al. 2002; Shellnutt 2013). Some of the associated mafic-ultramafic intrusions host world-class Fe-Ti-V oxide ore deposits or economically valuable Ni-Cu-PGE sulfide deposits (Zhou et al.,2005; Song et al., 2013; Tao et al., 2007, 2008).

Many researchers have studied the genetic relationships between different types of lavas and the mineralized mafic-ultramafic intrusions (e.g., Wang et al. 2007; Zhou et al. 2008; Zhang et al. 2009; Song et al. 2009; Ma et al. 2009; Zhong et al. 2011). These studies show that the ore-bearing intrusions formed by basaltic magmas in the upper crust and that the basalts are the derivatives of mantle-derived magmas by fractional crystallization (e.g., Tao et al. 2008, 2010; Pang et al. 2009; Song et al. 2013). However, the depths of fractional crystallization are yet to be determined. In this paper, we use phenocryst compositions as well as olivine-liquid thermometer and a clinopyroxene-liquid thermobarometer (Putirka et al. 1996; Putirka 2008) to estimate P and T conditions of crystallization. We then use the results to reconstruct the magma

plumbing system of the large igneous province.

Geological background

The ELIP exposes outcrops of a wide variety of rocks including mafic-ultramafic intrusions and volcanic rocks such as picrites and basalts. The intrusive and extrusive rocks are coeval and genetically related by differentiation at depths (Tao et al. 2010 Zhou et al. 2008; Song et al. 2013). In the western part of the Yangtze block there are large volume Emeishan Continental Flood Basalts (ECFB) and associated mafic-ultramafic intrusions which were erupted and emplaced in Late Permian (Fig. 1). The volcanic succession covers an estimated area of 3×10^5 km^2, with thicknesses ranging from several hundred meters up to 5 km (Xu et al. 2001; Song et al. 2001). The ECFB is recognized as one of the largest igneous provinces in the world and probably represents the product of a mantle plume (Chung and Jahn 1995; Xu et al. 2004), which we will test by estimating mantle potential temperatures. The volcanic succession overlies Early Permian limestone of the Maokou Formation, and is overlain by sandstone of the late Permian Xuanwei Formation. Zircon U-Pb dating of many mafic-ultramafic intrusions constrains the age of the ELIP at ~260 Ma, synchronous with the end-Guadalupian mass extinction (Zhou et al. 2002; Fan et al. 2008; Tao et al. 2009).

According to the classification of Xu et al. (2001), the volcanic rocks of the ELIP belong to either the high-Ti or low-Ti series based on whole-rock TiO_2 contents and Ti/Y ratios (e.g., Xu et al. 2001; Wang et al. 2010a). The high-Ti series is defined as that with TiO_2 >2.5 wt.% and Ti/Y>500, whereas the low-Ti series is defined as that with TiO_2 < 2.5 wt.% and Ti/Yb<500.

Rare picrites have been found mainly in the west (Dali, Lijiang, Binchuan, Yongsheng, Ertan, Muli) and in the south (Jinping-Song Da). They are interbedded with basaltic flows and vary in composition from Nb-depleted, low-Ti picrites to Nb-enriched, high-Ti picrites (Zhang et al. 2006a; Zhou et al. 2008; Hanski et al. 2010; Li et al. 2012). Cognate olivine phenocrysts in picrites have high Ca contents up 0.50 wt %, Fo contents up 92 mole %. These olivines are likely phenocrysts and indicates a MgO content of >20 wt.% for the parental melt, similar to the composition of primary mantle-derived magmas found elsewhere (Zhang et al. 2006a, 2006b; Hanski et al. 2010; Li et al. 2012; Kamenetsky et al. 2012). Most researchers agree that the picritic melts represent the parents of the associated low-Ti and high-Ti flood basalts. The basaltic magmas are thought to be developed in staging areas (magma chambers) by crystal fractionation, magma mixing and crustal contamination (Zhang et al. 2006a, 2008b; Hanski et al. 2010; Li et al. 2012; Kamenetsky et al. 2012; Howarth and Prevec 2013; Shellnutt and Wang 2014), though it is unclear at what depth the magma chambers are located.

Mafic and mafic-ultramafic intrusions are exposed mainly in a belt extending along the Panzhihua-Xichang region (Kangdian axis) from north in Danba to the south in Yunan and along the Red River (Honghe) fault, due to severe post-emplacement uplifting and erosion (Fig. 1). Two types of mineral deposits are associated with the intrusions: relatively smaller and more primitive intrusions contain Ni-Cu-PGE sulfide mineralization, whereas some of the larger and more evolved intrusions host giant Fe-Ti-V oxide deposits (Zhou et al. 2005, 2008; Zhong et al. 2006; Wang et al. 2008; Song et al. 2008; Zhang et al. 2009; Luo et al. 2014). Zhou et al. (2008) noted that the oxide-bearing intrusions are characterized by spiderdiagrams displaying positive Nb- and

Ti-anomalies and in certain cases negative Zr-Hf anomalies, whereas the sulfide-bearing intrusions have obvious negative Nb- and Ti-anomalies. So, it is believed that the oxide-bearing gabbroic intrusions were derived from high-Ti series magma whereas the sulfide-bearing mafic-ultramafic intrusions were derived from low-Ti series magmas (Zhou et al. 2008; Wang et al. 2010).

The Ni-Cu-PGE sulfide deposits associated with the mafic-ultramafic intrusions and bulk sulfides are widely variable in composition ranging from PGE-rich to PGE-poor (Song et al. 2008). The Jinbaoshan Pt-Pd deposit and the Limahe Ni-Cu sulfide deposit are two representative end-members in the ELIP: the former represents a sulfide-poor PGE deposit; the later is the best example of a sulfide-rich Ni-Cu deposit. The geology of the two deposits was described by Tao et al. (2007, 2008).

Magmatic Fe-Ti-V oxide deposits are documented in several layered intrusions in the Panzhihua-Xichang region (Fig. 1). Four major Fe-Ti oxide deposits including Panzhihua, Hongge, Baima and Xinjie account for a total ore reserve of ~7209 Mt total Fe, ~559 Mt TiO_2 and ~17.4 Mt V (Pang et al. 2008, 2010; Hou et al. 2013; Liu et al. 2014; Yu et al. 2015).

Petrography and analytical methods

Picrites and basalts

The picrite samples used in this study are from the Wumulaka area (East of Lijiang), and the Daying area (northeast of Dali) (Fig. 1). The picrites are spatially associated with basalts. The picrite and basalt samples were collected at different heights of 20 – 50m thick lava flows within a volcanic sequence that is >1 km thick. There are both high-Ti

and low-Ti picrites in Daying. Picrites found in Wumulaka belong to the high-Ti series. Most picrites are porphyritic with 10 – 30 % olivine phenocrysts, and a few samples, such as DY1-1, contain up to 50 % olivine phenocrysts. Two series of picrites are distinguished on the basis of petrography: high-Ti picrites are more clinopyroxene-rich, having anywhere from equal to even more clinopyroxene phenocrysts compared to olivine phenocrysts; in some of these samples we have found clinopyroxene phenocrysts that are as large as 2 mm x 5 mm (Fig. 2a). Low-Ti picrites, in contrast, contain few clinopyroxene phenocrysts; olivine phenocrysts are dominant and rare clinopyroxene phenocrysts are generally <2 mm (Fig. 2b). Euhedral chromite occurs mainly as inclusions in olivine as described in Li et al. (2008), and must have crystallized together with or before at least some of the olivine crystallized. Olivine phenocrysts from the high-Ti picrites have Fo contents ranging from 80 to 90 mole % but ranging to as low as Fo73 in a few samples. Olivine phenocryts from low-Ti picrites have Fo contents ranging from 84 to 93 mole %. Olivine phenocrysts of variable sizes are partially altered to serpentine in the margins and micro-fractures. Micro-crystals of pyroxenes and plagioclase in the groundmass are partially altered to chlorite, talc and clay minerals.

Basalts are the predominant volcanic rock type of the ELIP, covering an area of $>3\times10^5$ km^2 in SW China, with total thicknesses varying from several hundred up to 5000 meters**.** These successions are described by Xu et al. (2001). The ELIP basalts have <8 wt. % MgO and relatively low Ni contents (<100 ppm).

Basalts in the ELIP are varied and include pyroxene-phyric basalts, plagioclase-phyric basalts, amygdaloidal basalts, and aphyric basalts. Pyroxene-phyric basalts are widespread in the ELIP and are found in most volcanic successions. The

samples of pyroxene-phyric basalts in this study have been collected from Daying (Bingchuan), and Wumulaka (Yongsheng) in Yunnan, and Ertan, Longzhushan in Sichuan, Liupanshui, and Heshitou in Guizhou (Fig. 1). They have <3 – 5 % clinopyroxene phenocrysts; the fine-grained groundmass has intergranular to massive textures (Fig. 2c, d). High-Ti and low-Ti basalts cannot be distinguished petrographically, but are only distinguished based on whole-rock TiO_2 contents and Ti/Y ratios (e.g., Xu et al. 2001; Qi and Zhou 2008).

Sample analysis

Compositions of olivine and clinopyroxene were determined by wavelength-dispersive X-ray emission microanalysis using a CAMECA SX50 electron microprobe at the Department of Geological Sciences, Indiana University. The analytical conditions for major elements were 15 kV, 20 nA beam current, 1 μm beam size and peak-counting time of 20 seconds. Minor and trace elements such as Cr, Ti, V and Ni were analyzed using a beam current of 100 nA and a peak-counting time of 50 seconds. The detection limits for these elements under such conditions are ~100 ppm. Raw data were corrected using the PAP program supplied by CAMECA. Analytical reproducibility is ±2 %. The accuracy of the analyses was monitored using mineral standards. Samples include two series of picrites and basalts in the ELIP (Appendix 1 of supplementary).

Whole rock major element compositions of corresponding samples were determined by XRF using an AXIOS-PW4400 wavelength dispersive spectrometer at the Institute of Geochemistry, Chinese Academy of Sciences, Guiyang (Appendix 1 of supplementary).

Mineral-liquid equilibrium tests

According to partition coefficients of $K_D(Fe\text{-}Mg)^{ol\text{-}liq}$ and $K_D(Fe\text{-}Mg)^{cpx\text{-}liq}$, we could test the equilibrium state of clinopyroxene and olivine with their whole rock hosts.

Equilibrium state of olivine phenocrysts: In the Rhodes Diagrams for olivines (Fig.3 a), the solid and dashed lines in Fig.3a represent a $K_D(Fe\text{-}Mg)^{ol\text{-}liq}$ value of 0.31 ± 0.03, close to the value of Roeder and Emslie (1970; 0.30) although slightly higher, but likely appropriate given experimental work by Herzberg and O'Hara (1997) and Matzen et al. (2011). We find that, olivines in picrites studied here have a wide variation in composition (Fo) even in a single sample,. Most olivines are not in equilibrium with their whole rock hosts, but maximum Fo contents are consistent with equilibrium, and hence consistent with closed system fractionation. This test indicates that most high Fo olivines are most likely phenocrysts, precipitated from a liquid that approximates the whole rock in composition. Olivines with lower Fo contents clearly crystallized from evolved magmas, perhaps related to the whole rock, but also quite possibly related to prior intrusions and episodes of olivine crystallization.

Equilibrium state of clinopyroxene phenocrysts: By using the $K_D(Fe\text{-}Mg)^{cpx\text{-}liq}$ = 0.27± 0.03 (Villiger et al., 2007), the Rhodes Diagram for clinopyroxene is shown in figure 3b. We found that all the clinopyroxene phenocrysts, including the maximum Mg# clinopyroxene in picrites are not in equilibrium with their whole rock hosts. This could be thought as that the clinopyroxene in picrites crystallized after most olivine crystallized. The whole rock has much higher Mg# than clinopyroxene-equilibrated liquid due to olivine accumulation in the rock.

Thermobarometric calculations

Methods

Estimating T from Olivine-Liquid Thermometry: There exists a large number of olivine geothermometers. Most recent interest in olivine thermometry has revolved about the partitioning of Mg between olivine and liquid (e.g., Ford et al. 1983; Beattie 1993; Herzberg and O'Hara 2002; Falloon et al. 2007; Putirka, 2007). Putirka et al. (2008) had reviewed those published models of olivine-liquid thermometers based on Mg partitioning. The review shows that the model developed by Putirka et al. (2007) (their Equation 4) and Beattie (1993) are best and recover experiments with standard errors of estimate in ± 43 K (Putirka et al. 2008). We use the olivine-liquid based thermometer of Putirka et al. (2007), their Equation 4 (which is the same as Eqn. 22 in Putirka 2008) for temperature estimates, since it accounts for water contents in magmas, whereas the Beattie (1993) model is only applicable for dry systems. It uses the composition of olivine and coexisting liquid to determine the temperature at which these two phases were last in equilibrium.

Equationn. 22 in Putirka 2008 is pressure dependent. According to pressure estimation of clinopyroxene in picrites later (the most high pressure is about 1.0 GPa) and Considering how density influences magma ascent, it is supposed that most olivines in picrites are crystallized in depth from the Moho to middle crust (see Putirka et al. 2009; Putirka 2008). We thus assume for the ol-liquid geothermometer that P = 1.3 GPa as appropriate input in the calculation.

Estimating P and T using Clinopyroxene-based Thermobarometer: Clinopyroxene has received much attention in estimation of magma crystallization depths

for volcanic rocks due to its notable sensitivity to P. Many workers developed thermometers and barometers based on clinopyroxene compositions alone (Nimis 1995; Nimis and Ulmer 1998), or clinopyroxene-liquid equilibria (Putirka et al. 1996, 2003, 2008). Our calculations for clinopyroxene pressures and temperatures make use of the models developed by Putirka et al. (2008), their Eqn.30 for pressure and Eqn.33 for temperature, which employs the compositions of coexisting liquid and clinopyroxene compositions and is to be preferred for basaltic and picritic compositions. Comparing with previous wide used models of the Jd-DiHd exchange thermometers (Putirka et al. 1996), the new calibrated models are expected to reduce uncertainties by about 10-20 °C in temperature and about 3-4 Kb in pressure from global calibrations. Equation 30 in Putirka (2008) was calibrated using a wide experimental data set, and the standard errors of estimate are ±1.6 Kb (Putirka et al. 2008). Equation 33 is developed based on global calibrations using experiments conducted at P < 70 Kb, and the standard error of estimate is ± 45 K (Putirka et al. 2008). As a check, we use equations P1 and T1 from Putirka et al. (1996).

Liquid equilibrated with olivine and clinopyroxene

As noted above, the maximum Fo content olivines are in equilibrium with whole rocks, but clinopyroxnes are not. For this reason, we pair maximum Fo content olivnes with whole rock compositions to obtain ol-liq temperatures, but we make compositional corrections before applying thermobarometers.

Liquid equilibrated with olivine in picrites: Based on Rhodes Diagrams for olivine (Fig.3a), it is reasonable to assume the Kd=0.31 in the olivine-melt equilibrium

for our studied picrites. By using $Kd^{(Fe\text{-}Mg)}_{cpx\text{-}liq}$=0.31 as an appropriate value, we estimate and subtract the fraction of extra previous crystallized olivine from the whole rock to obtain the liquid composition equilibrated with the observed Fo olivine.

Liquid composition equilibrated with clinopyroxene in picrites: To test whether it is possible to obtain a liquid in equilibrium with observed cpx, we begin by removing previously crystallized olivine from the whole rock unitl $K_D(Fe\text{-}Mg)^{cpx\text{-}liq} = 0.27$. We then check whether the amount of olivine that is removed to obtain this value is equal to or less than observed olivine modes. We find that removal of X% olivine on average allows us to achieve liquid compositions that are in equilibrium with observed clinopyroxene, which is less than observed modal amounts of olivine in the whole rocks.

Liquid composition equilibrated with clinopyroxene in basalts: Based on the Rhodes Diagram for clinopyroxene (Fig.3b), clinopyroxene in basalts are allowably in equilibrium with liquids that approximate of whole rock compositions. So, we pair the whole rock composition with the clinopyroxene in basalts.

The liquids composition equilibrated with clinopyroxene and olivine in picrites and basalts are provided in Appendix 2 of Supplementary.

H_2O in melt liquids

Another factor that influences mineral-liquid equilibration is water in magmas. Although water contents measurement in melt inclusions show wide variability (Humphreys et al. 2008; Esposito et al. 2014), studies of hotspot basalts have come to the conclusion that mantle plumes have higher H_2O abundances compared to MORB (Hauri 2002). Water abundances measured in Hawaiian melt inclusions ranges in 0.03–0.84

wt.% (Hauri, 2002). There is 0.25-0.69 % water in basaltic glasses at Kerguelen plateau (Wallace 2002). Some hotspots, such as Yellowstone, have extremely high water with maximum concentrations of 3.3 wt% observed in olivine-hosted melt inclusions, and may be influenced by subduction (Stefano et al. 2011). In our study, since mineral melt inclusion H_2O estimates are absent at the ELIP, we assume that H_2O is 0.3% for picrites and 0.7 % for basalts, simiar to non-subduction related plumes.

Results

Olivine - Liquid Temperatures Estimates: Results of our thermometry are shown in Figure 4 and Appendix 3 of the Supplementary Files. Temperatures for of olivine crystallization are as follows: low-Ti picrites: 1536 –1296°C; high-Ti picrites: 1462 – 1241°C (mostly). Mantle potential temperature (T_p) estimates carry significant uncertainty, since (a) our observed $K_D(\text{Fe-Mg})^{\text{ol-liq}} = 0.31$, but according to Matzen et al (2011), $K_D(\text{Fe-Mg})^{\text{ol-liq}}$ may be as high as 0.35, and (b) due to uncertainty in estimates of melt fraction (F), which for the low-Ti suite are in the range 0.32-0.36 using models from Putirka et al. (2007). If we allow that F may be as low as 0.2, then T_p for the low-Ti suite is in the range 1740-1810 ^{o}C, significantly higher than at Hawaii (Putirka et al. (2007), and also higher than other Cretaceous LIPs from Herzberg and Gazel (2009). The high-Ti parental magmas yield much cooler estimates, with T_p in the range 1510-1610^{o}C, with F predicted to be between 0.09 and 0.17 and a liquid in equilibrium with Fo91 in the mantle source region. Either of these estimates is significantly high enough to characterize the Emeishan ELIP as a mantle plume.

Clinopyroxene--liquid P-T estimates: As shown in Figure 5 and Appendix 3, our

thermobarometric calculations show that the dominant crystallization depths of clinopyroxene phenocrysts in the picrites are ~ 25 km, with temperatures in the range of 1190 to 1275°C. The clinopyroxene phenocrysts in the associated basalts yield lower crystallization depths, <20 km, with temperatures in the range of 1094 to 1214°C.

It is useful to compare the estimated crystallization depths with the crustal structure of the Yangtze craton. Geophysical data reveal that the upper, middle and lower crust boundaries in the western Yangtze craton where the ELIP occurs are located at respective depths of 16 km, 33 km and 55 km below the surface (Jiang et al. 2012). The estimated clinopyroxene crystallization depths for the Emeishan picrites correspond to depths of the middle crust. The estimated clinopyroxene crystallization depths for the associated basalts correspond the depths of the upper crust.

Discussion

Density influence on magma storage and ascent

Magma transport and storage are influenced by density variations (Stolper and Walker, 1980). Ascent may cease temporarily or permanently at a level of neutral buoyancy where magma density equals that of the host rock and buoyancy becomes zero (Ryan 1987; Lister and Kerr 1991). Here, magma densities are calculated from the models of Lange and Carmichael (1990) and Ochs and Lange (1999), using liquid compositions which are equilibrated with Cpx and P-T conditions from clinopyroxene-melt thermobarometers. The results are listed in Appendix 3 of Supplementary.

The highest Fo olivine (Fo=92.5) in our study is from sample DY8-8, and is among

the highest Fo olivines ever recorded in the entire ELIP (Zhang et al. 2006a; Hanski et al. 2010; Kamanetsky et al. 2012; Li et al. 2012). More important, by all appearances it is in equilibrium with the liquid that has a composition of the whole rock (Fig. 3b). So, the whole rock composition of sample DY8-8 is assumed to represent a parental, mantle-derived magma in ELIP. The density of this primary magma (in composition of whole rock sample DY8-8) in the Moho is about 3.0 g/cm^3 calculated by assuming temperature is 1500°C and pressure is 16 Kbar in depth of 55 Km.

Calculations of liquid density, in comparison to crustal density show that the primary mantle-derived magma before undergoing differentiation are positively buoyant in the mantle but negatively buoyant at the Moho and at all crustal depths above the Moho (Fig. 6). Perhaps without a trans-lithospheric fault-controlled conduit such magmas would be permanently trapped here, rather than erupted. Our calculations also show that fractionated magmas are negatively buoyant in the middle and upper crusts but have densities that are less than the lower crust (Fig. 6), which is consistent with the density trap model of Kuntz (1992) and Putirka et al. (2009). This, together with the depths of crystallization estimated from clinopyroxene phenocrysts in the lavas, allow us to posit that the ELIP fractionated magmas were once trapped in the middle or upper crust.

Magma plumbing system in the ELIP

It is posited that magmas move *via* fracture transport and/or magma fracture, creating a plumbing structure on their way toward the surface (Ryan 1987, 1988; Cox 1993; Putirka and Condit 2003, Valentine and Gregg 2008; Ferlito et al. 2014). Pressures of crystallization estimated from igneous thermobarometers can be translated into magma

staging depths and so they are widely used to constrain magma transport and storage (e.g., Putirka 1997, 2005; Schwarz et al. 2004; Klügel et al. 2005; Galipp et al. 2006; Mordick and Glazner 2006; Dahren et al. 2012; Keiding et al. 2013; Larsen et al. 2013; Mollo et al. 2013).

Pressures and T estimated using clinopyroxene-based thermobarometers, plus the density influence described above, allow us to reconstruct the magma plumbing system of the ELIP (Fig. 7). The proposed magma plumbing system consists of a source mantle, three major staging chambers and various conduits reaching at different depths to extract magma from the staging chambers. The primary mantle-derived magmas may have ascended directly from the Moho, or perhaps even from below the Moho, to the surface *via* concurrent trans-lithosphere fault-controlled conduits, although such deep conduits are extremely difficult to create and maintain due to increasing lithostatic-pressure with depth. Mantle-derived magmas, or fractionated picrites, appear to reach the middle and upper crusts, undergoing further crystallization and crustal contamination. Some of the evolved magmas eventually erupt to the surface to form the volcanic rocks, also via trans-crust fault-controlled conduits. In this model, the coeval mafic-ultramafic intrusions in the upper crust are thought to represent the cumulates of the evolving magmas in some of the staging chambers.

Petrogenetic implications

There are several important petrogenetic implications from the results of this study. Firstly, the popular interpretation that the Ni-Cu-(PGE) sulfide ore-bearing mafic-ultramafic intrusions and the Fe-Ti-V oxide ore-bearing gabbroic intrusions, which

occur in the upper crust and are coeval with the Emeishan flood basalts, are subvolcanic intrusions (e.g. Li et al. 2003, 2009; Arndt et al. 2005; Barnes and Lightfood 2005; Naldrett 2010; Song et al. 2013; Tang et al. 2013), is supported by our observation that the coeval flood basalts were indeed once stored in the upper crust. Secondly, variable differentiation of mantle-derived magma is facilitated by a complex magma plumbing system with multiple storage reservoirs at different depths. Finally, picrites are rare and basalts are dominant in a continental flood basalt province such as Emeishan because more primitive magmas tend to be trapped at greater depth than more evolved magma and because deeper conduits are more difficult to create and maintain due to increasing lithospheric pressure with depth.

Implications

Several important conclusions can be drawn from this study. These are listed below.

(1) Pressures of crystallization estimated from igneous thermobarometers involving clinopyroxene phenocrysts can be used to determine the magma staging depths of continental flood basalt province such as Emeishan.

(2) The magma storage reservoirs of the Emeishan flood basalts occur in the middle and upper crusts at ~25 km and <20 km, respectively.

(3) Picrites are rare in the Emeishan food basalt province because the majority of primary magma from the mantle was trapped in the staging chambers, undergoing crystal fractionation and crustal contamination.

(4) The estimated crystallization depths of clinopyroxene phenocrysts in the Emeishan basalts provide another support for the notion that some of the coeval

mafic-ultramafic intrusions in the underlying upper crust are indeed the conduits of the lavas.

(5) Mantle potential temperature estimates for low-Ti picrites are the highest yet recorded for lavas erupted at any age, and certainly since the Cretaceous, and should impact how we view secular cooling rates.

Acknowlegements

We thank Prof. Ian Swainson for revision guidance and Prof. Madeleine Humphreys, Massimo D'Antonio for their constructive comments and useful suggestions. This study was supported by CAS/SAFEA International Partnership Program for Creative Research Teams (KZZD-EW-TZ-20), the National 973 Program of China (2012CB416804 and 2014CB440906) and National Natural Sciences Foundations of China (40973039).

Supplementary Materials

Appendix 1~ 3 as Supplementary Materials associated with this article can be found in the online version.

References cited

Arndt, N.T., Lesher, C.M., and Czamanske, G.K. (2005) Mantle-derived magmas and magmatic Ni-Cu-(PGE) deposits. Economic Geology, 100, 5–23.

Bai, Z.J., Zhong, H., Naldrett, A.J., Zhu, W.G., and Xu, G.W. (2012) Whole-rock and mineral composition constraints on the genesis of the giant Hongge Fe-Ti-V oxide

deposit in the Emeishan Large Igneous Province, Southwest China. Economic Geology, 107, 507–524.

Bai, Z.-J., Zhong, H., Li, C., Zhu, W.-G., He, D.-F., and Qi, L. (2014) Contrasting parental magma compositions for the Fe-Ti-V oxide ore-bearing horizons of the Hongge and Panzhihua intrusions, Emeishan large igneous province, SW China. Economic Geology, 109, 1763–1785.

Barnes, S.-J., and Lightfood, P.C. (2005). Formation of magmatic nickel sulfide ore deposits and processes affecting their copper and platinum group element contents. Economic Geology, 100, 179–213.

Beattie, P. (1993) Olivine-melt and orthopyroxene-melt equilibria. Contributions to Mineralogy and Petrology, 115, 103-111.

Chung, S.L., and Jahn, B.M. (1995) Plume-lithosphere interaction in generation of the Emeishan flood basalts at the Permian-Triassic boundary. Geology, 23, 889–892.

Cortes, J.A., Smith, E.I., and Valentine, G.A. (2015) Intrinsic conditions of magma genesis at the Lunar Crater Volcanic Field (Nevada), and implications for internal plumbing and magma ascent. American Mineralogist, 100(2-3), 396-413.

Courtillot, V., Jaupart, C., Manighetti, I, Tapponnier, P., and Besse, J. (1999) On causal links between flood basalts and continental breakup. Earth and Planetary Science Letters, 166, 177–195

Cox, K.G. (1993) Continental magmatic underplating, in K.G. Cox, D. McKenzie, R.S. White, Ed., Melting and Melt Movement in the Earth, p. 155–166. Oxford University Press, Oxford.

Dahren, B., Troll V.R.,Andersson U.B., Chadwick, J.P., Gardner, M.F., Jaxybulatov, K.,

and Koulakov, I. (2012) Magma plumbing beneath Anak Krakatau volcano, Indonesia: evidence for multiple magma storage regions. Contributions to Mineralogy and Petrology,163, 631–651.

Esposito, Rosario; Hunter, Jerry; Schiffbauer, James, D. (2014) An assessment of the reliability of melt inclusions as recorders of the pre-eruptive volatile content of magmas. American Mineralogist, 99(5-6), 976-998.

Falloon, T. J., Danyushevsky, L. V., Alexei, A., Green, D. H., and Ford, C. E. (2007) The application of olivine geothermometry to infer crystallization temperatures of parental liquids: Implications for the temperature of MORB magmas. Chemical Geology, 241, 207–233.

Fan, W.M., Zhang, C.H., Wang, Y.J., Guo, F., and Peng, T.P. (2008) Geochronology and geochemistry of Permian basalts in western Guangxi Province, Southwest China: Evidence for plume-lithosphere interaction. Lithos, 102, 218–236.

Ferlito, C., Coltorti, M., Lanzafame, G., and Giacomoni, P.P. (2014) The volatile flushing triggers eruptions at open conduit volcanoes: Evidence from Mount Etna volcano (Italy). Lithos, 184–187, 447–455.

Ford, C.E., Russell, D.G., Craven, J.A., and Fisk, M.R.(1983) Olivine-liquid equilibria: temperature, pressure and composition dependence of the crystal/liquid cation partition coefficients for Mg, Fe2+, Ca and Mn. Journal of Petrology, 24, 256–265

Galipp, K., Klügel, A., and Hansteen, T.H. (2006) Changing depths of magma fractionation and stagnation during the evolution of an oceanic island volcano: La Palma (Canary Islands). Journal of Volcanology and Geothermal Research, 155, 285–306.

Gao, S., Luo, T.-C., Zhang B.-R., Zhang H.-F., Han Y.-W., Hu Y.-K., and Zhao Z.-D. (1998) Chemical composition of the continental crust as revealed by studies in east China. Geochimica et Cosmochimica Acta, 62, 1959–1975.

Hanski, E., Kamenetsky, V.S., Luo Z.-Y., Xu Y.-G., and Kuzmin, D.V. (2010) Primitive magmas in the Emeishan Large Igneous Province, southwestern China and northern Vietnam. Lithos, 119, 75–90.

Hauri, E. (2002) SIMS analysis of volatiles in silicate glasses, 2: isotopes and abundances in Hawaiian melt inclusions. Chemical Geology, 183(1–4), 115–141.

Herzberg, C.T., and Gazel, E. (2009) Petrologicla evidence for secular cooling in the mantle. Nature, 458, 619-623.

Herzberg, C.T, and O'Hara, M.J. (2002) Plume-associated ultramafic magmas of Phanerozoic Age. Journal of Petrology, 43, 1857–1883.

Herzberg, C.T., and Zhang, J. (1997) Melting experiments on komatiite analogue compositions at 5 GPa. American Mineralogist, 82, 354–367.

Hou, T., Zhang, Z., Encarnacion, J., Santosh, M., and Sun, Y. (2013) The role of recycled oceanic crust in magmatism and metallogeny: Os-Sr-Nd isotopes, U-Pb geochronology and geochemistry of picritic dykes in the Panzhihua giant Fe-Ti oxide deposit, central Emeishan large igneous province, SW China. Contributions to Mineralogy and Petrology, 165, 805–822.

Howarth, G.H., and Prevec, S.A. (2013) Trace element, PGE, and Sr–Nd isotope geochemistry of the Panzhihua mafic layered intrusion, SW China: Constraints on ore-forming processes and evolution of parent magma at depth in a plumbing-system. Geochimica et Cosmochimica Acta, 120, 459–478

Humphreys, M.C.S., Menand T., Blundy, J.D., and Klimm, K. (2008) Magma ascent rates in explosive eruptions: Constraints from H_2O diffusion in melt inclusions. Earth and Planetary Science Letters, 270, 25–40.

Jiang, W., Zhang, J., Tian, T., and Wang, X. (2012) Crustal structure of Chuan-Dian region derived from gravity data and its tectonic implications. Physics of the Earth and Planetary Interiors, 212–213, 76–87.

Kamenetsky, V.S., Chung S.-L., Kamenetsky M., and Kuzmin D.V. (2012) Picrites from the Emeishan Large Igneous Province, SWChina: a Compositional Continuum in Primitive Magmas and their Respective Mantle Sources. Journal of Petrology, 53(10), 2095–2113

Keiding, J.K., Frei, O., Renno, A.D., Veksler, I.V., and Trumbull R.B. (2013) Conditions of magma crystallization in the Henties Bay-Outjo dyke swarm, Namibia: Implications for the feeder system of continental flood basalts. Lithos, 179, 16–27.

Klügel, A., Hansteen, T.H., and Galipp, K. (2005) Magma storage and underplating beneath Cumbre Vieja volcano, La Palma (Canary Islands). Earth and Planetary Science Letters, 236, 211–226.

Kuntz, M. A. (1992) A model-based perspective of basaltic volcanism, eastern Snake River Plain, Idaho. In: P. K., Link, M.A. Kuntz, and L.B. Platt, Ed., Regional Geology of Eastern Idaho and Western Wyoming, 179, p. 289–304. Geological Society of America, Memoirs.

Lange, R.L. and Carmichael, I.S.E. (1990) Thermodynamic properties of silicate liquids with emphasis on density, thermal expansion and compressibility. In J. Nicholls, and J. K. Russell, Ed., Modern Methods of Igneous Petrology, 24, p. 25–64. Reviews in

Mineralogy, Mineralogical Society of America.

Larsen, J.F., Śliwiński, M.G., Nye, C., Cameron, C., and Schaefer, J.R. (2013) The 2008 eruption of Okmok Volcano, Alaska: Petrological and geochemical constraints on the subsurface magma plumbing system. Journal of Volcanology and Geothermal Research, 264, 85–106.

Li, C., Ripley, E.M., and Naldrett, A.J. (2003) Compositional variations of olivine and sulfur isotopes in the Noril'sk and Talnakh intrusions: Implications for ore forming processes in dynamic magma conduits. Economic Geology, 98, 69–86.

Li, C., Ripley, E.M., Tao, Y., and Mathez, E.A. (2008) Cr-spinel/olivine and Cr-spinel/liquid nickel partition coeffcients from natural samples. Geochimica et Cosmochimica Acta, 72, 1678–1684.

Li, C., Ripley, E.M., and Naldrett, A.J. (2009) A new genetic model for the giant Ni-Cu-PGE sulfide deposits associated with the Siberian flood basalts. Economic Geology, 104, 291–301.

Li, C., Tao, Y., Qi, L., and Repley, E.M. (2012) Controls on PGE fractionation in the Emeishan picrites and basalts: Constraints from integrated lithophile-siderophile elements and Sr-Nd isotopes. Geochimica et Cosmochimica Acta, 90, 12–32.

Lister, J.R., and Kerr, R.C. (1991) Fluid-mechanical models of crack propagation and their application to magma transport in dykes. Journal of Geophysical Research, 96 (B6), 10049–10077.

Liu, P.-P., Zhou, M.-F., Wang, C.Y., Xing, C.-M., and Gao J.-F. (2014) Open magma chamber processes in the formation of the Permian Baima mafic-ultramafic layered intrusion, SW China. Lithos, 184–187, 194–208.

Luo, W., Zhang, Z., Santosh, M., Hou, T., Huang, H., Zhu, J., Wang, X., and Fu, X. (2014) Petrology and geochemistry of Permian mafic-ultramafic intrusions in the Emeishan large igneous province, SW China: Insight into the ore potential. Ore Geology Reviews, 56, 258–275.

Ma, Y.-S., Tao, Y., Zhong, H., Zhu, F.-L, Zhou, J.-X. (2009) Geochemical characteristics of platinum-group elements in Abulangdang ultramafic intrusion, Sichuan Province, China. Chinese Journal of Geochemistry (English Edition), 28(3), 320–327.

Matzen, A. K., Bajer, M. B., Beckett, J. R. and Stolper, E. M. (2011) Fe^Mg partitioning between olivine and high-magnesian melts and the nature of Hawaiian parental liquids. Journal of Petrology. 52(7-8), 1243-1263.

Mollo, S., Putirka, K., Misiti, V., Soligo, M., and Scarlato, P. (2013) A new test for equilibrium based on clinopyroxene–melt pairs: Clues on the solidification temperatures of Etnean alkaline melts at post-eruptive conditions. Chemical Geology, 352, 92–100.

Mordick, B.E., and Glazner, A.F. (2006) Clinopyroxene thermobarometry of basalts from the Coso and Big Pine volcanic fields, California. Contributions to Mineralogy and Petrology, 152, 111–124.

Naldrett, A.J. (2010) From the mantle to the bank: The Life of a Ni-Cu-(PGE) Sulfide deposit. South African Journal of Geology, 113(1), 1–32.

Nimis, P. (1995) A clinopyroxene geobarometer for basaltic systems based on crystals-structure modeling. Contributions to Mineralogy and Petrology, 121:115-125.

Nimis, P., and Ulmer, P. (1998) Clinopyroxene geobarometry of magmatic rocks.

Part 1: an expanded structural geobarometer for anhydrous and hydrous basic and ultrabasic systems. Contributions to Mineralogy and Petrology, 133, 122-135.

Ochs, F. A., and Lange, R.A. (1999). The density of hydrous magmatic liquids. Science, 283, 1314 – 1317.

Pang, K.N., Li, C., Zhou, M.-F., and Ripley, E.M. (2008) Abundant Fe–Ti oxide inclusions in olivine from the Panzhihua and Hongge layered intrusions, SW China: evidence for early saturation of Fe-Ti oxides in ferrobasaltic magma. Contributions to Mineralogy and Petrology, 156, 307–321.

Pang, K.N., Li, C., Zhou, M.-F., and Ripley, E.M. (2009) Mineral compositional constraints on petrogenesis and oxide ore genesis of the late Permian Panzhihua layered gabbroic intrusion, SW China. Lithos, 110, 199–214.

Pang, K.-N., Zhou, M.-F., Qi, L., Shellnutt, G., Wang, C.Y., and Zhao, D. (2010) Flood basalt-related Fe-Ti oxide deposits in the Emeishan large igneous province, SW China. Lithos, 119, 123–136.

Putirka, K. (1997) Magma transport at Hawaii: inferences from igneous thermobarometry. Geology, 25, 69–72.

Putirka, K. (2008). Thermometers and barometers for volcanic systems. In K. D. Putirka, and F. Tepley, Ed., Minerals, Inclusions and Volcanic Processes. 69, p. 61–120. Reviews in Mineralogy and Geochemistry, Mineralogical Society of America and Geochemical Society.

Putirka, K., and Condit, C. (2003) A cross section of a magma conduit system at the margins of the Colorado Plateau. Geology, 31, 701–704.

Putirka, K., Johnson, M., Kinzler, R., and Walker, D. (1996) Thermobarometry of mafc

igneous rocks based on clinopyroxene-liquid equilibria, 0-30 kbar. Contributions to Mineralogy and Petrology, 123, 92–108.

Putirka, K., Perft, M., Ryerson, F.J., and Jackson, M.G. (2007) Ambient and excess mantle temperatures, olivine thermometry, and active vs. passive upwelling. Chemical Geology, 241, 177–206.

Putirka, K., Kuntz, M., Unruh, D., and Vaid, N. (2009) Magma evolution and ascent at the Craters of the Moon and neighboring volcanic fields, southern ID, USA: implications for the evolution of polygenetic and monogenetic fields. Journal of Petrology, 50, 1639–1665.

Qi, L., and Zhou, M.-F. (2008). Platinum-group elemental and Sr-Nd-Os isotopic geochemistry of Permian Emeishan flood basalts in Guizhou Province, SW China. Chemical Geology, 248, 83–103.

Roeder, P.L. and Emslie, R.F. (1970) Olivine-liquid equilibrium. Contributions to Mineralogy and Petrology, 71, 257–269.

Ryan, M.P. (1987) Neutral buoyancy and the mechanical evolution of magmatic systems. In B.O. Mysen, Ed., Magmatic Processes: Physicochemical Principles, Special Publication, 1, p. 259–287. The Geochemical Society, University Park, Texas.

Ryan, M.P. (1988) The mechanics and three-dimensional internal structure of active magmatic systems: Kilauea volcano, Hawaii. Journal of Geophysical Research, 93, 4213–4248.

Schwarz, S., Klügel, A., and Wohlgemuth-Ueberwasser, C. (2004) Melt extraction pathways and stagnation depths beneath the Madeira and Desertas rift zones (NE Atlantic) inferred from barometric studies. Contributions to Mineralogy and

Petrology, 147, 228–240.

Shellnutt, J.G. (2013) The Emeishan large igneous province: A synthesis. Geoscience Frontiers, 5(3), 369-394.

Shellnutt, J.G., and Wang, K.-L. (2014) An ultramafic primary magma for a low Si, high Ti-Fe gabbro in the Panxi region of the Emeishan large igneous province, SW China. Journal of Asian Earth Sciences, 79(A), 329–344

Song, X-Y., Zhou, M-F., Hou, Z.Q., Cao, Z.M., Wang Y.L, and Li, Y.G. (2001) Geochemical constraints on the mantle source of the Upper Permian Emeishan continental flood basalts, southwestern China. International Geology Review, 43, 213–225.

Song, X-Y., Zhou, M-F., Tao, Y., and Xiao, J.F. (2008) Controls on the metal compositions of magmatic sulfide deposits in the Emeishan large igneous province, SW China. Chemical Geology, 253, 38–49.

Song, X.Y., Qi, H.W., Hu, R.Z., Chen, L.M., Yu, S.Y., and Zhang, J.F. (2013) Formation of thick stratiform Fe-Ti oxide layers in layered intrusion and frequent replenishment of fractionated mafic magma: evidence from the Panzhihua intrusion, SW China. Geochemistry Geophysics Geosystems, 14, 712–732.

Stefano, C. J., Mukasa, S. B., Andronikov, A., and Leeman, W. P. (2011) Water and other volatile systematics of olivine-hosted melt inclusions from the Yellowstone hotspot track. Contributions to Mineralogy and Petrology, 161, 615–633.

Stolper, E., and Walker, D. (1980) Melt density and the average composition of basalt. Contributions to Mineralogy and Petrology, 74, 7–12.

Tang, Q., Ma, Y., Zhang, M., Li, C., Zhu, D., and Tao, Y. (2013) The Origin of

Ni-Cu-PGE Sulfde Mineralization in the Margin of the Zhubu Mafic-Ultramafic Intrusion in the Emeishan Large Igneous Province, Southwestern China. Economic Geology, 108, 1889–1901.

Tao, Y., Li, C., Hu, R., Ripley, E.M., Du, A.D., and Zhong, H. (2007) Petrogenesis of the Pt-Pd mineralized Jinbaoshan ultramafic intrusion in the Permian Emeishan Large Igneous Province, SW China. Contributions to Mineralogy and Petrology, 153, 321–337.

Tao, Y., Li, C., Song, X-Y., and Ripley, E.M. (2008) Mineralogical, petrological, and geochemical studies of the Limahe mafic-ultramatic intrusion and associated Ni-Cu sulfide ores, SW China. Mineralium Deposita, 43, 849–872.

Tao, Y., Ma, Y.S., Miao, L.C., and Zhu, F.L. (2009) SHRIMP U-Pb zircon age of the Jinbaoshan ultramafic intrusion, Yunnan Province, SW China. Chinese Science Bulletin (English Edition), 54, 168–172.

Tao, Y., Li, C., Hu, R., Qi, L., Qu, W., and Du, A. (2010) Re-Os isotopic constraints on the genesis of the Limahe Ni-Cu deposit in the Emeishan large igneous province, SW China. Lithos, 119, 137–146.

Valentine, G.A., and Gregg, T.K.P. (2008) Continental basaltic volcanoes-Processes and problems. Journal of Volcanology and Geothermal Research, 177, 857–873.

Villiger, S., Ulmer, P., and Müntener, O. (2007) Equilibrium and fractional crystallization experiments at 0.7 GPa; the effect of pressure on phase relations and liquid compositions of tholeiitic magmas. Journal of Petrology, 48, 159-184.

Wallace, P.J.(2002) Volatiles in submarine basaltic glasses from the Northern Kerguelen Plateau (ODP Site 1140): Implications for source region compositions, magmatic

processes, and plateau subsidence. Journal of Petrology, 43(7), 1311-1326.

Wang, C.Y., Zhou, M.-F., and Qi, L. (2007) Permian flood basalts and mafic intrusions in the Jinping (SW China)–Song Da (northern Vietnam) district: mantle sources, crustal contamination and sulfide segregation. Chemical Geology, 243, 317–343.

Wang, C.Y., Zhou, M.-F., and Zhao, D. (2008) Fe-Ti-Cr oxides from the Permian Xinjie mafic-ultramafic layered intrusion in the Emeishan large igneous province, SW China: crystallization from Fe- and Ti-rich basaltic magmas. Lithos, 102, 198–217.

Wang, C.Y., Zhou, M.-F., and Qi, L. (2010) Chalcophile element geochemistry and petrogenesis of high-Ti and low-Ti magmas in the Permian Emeishan large igneous province, SW China. Contributions to Mineralogy and Petrology, 161, 237–254.

Xu, Y.G., Chung, S.L., Jahn, B.M., and Wu, G.Y. (2001) Petrological and geochemical constraints on the petrogenesis of the Permo-Triassic Emeishan flood basalts in southwestern China. Lithos, 58, 145–168.

Xu, Y.G., He, B., Chung, S.L., Menzies, M.A., and Frey, F.A. (2004) Geologic, geochemical, and geophysical consequences of plume involvement in the Emeishan flood-basalt province. Geology, 32, 917–920.

Yu, S.-Y., Song, X.-Y., Ripley, E.M., Li, C., Chen, L.-M., She, Y.-W., and Luan, Y. (2015) Integrated O–Sr–Nd isotope constraints on the evolution of four important Fe–Ti oxide ore-bearing mafic–ultramafic intrusions in the Emeishan large igneous province, SW China. Chemical Geology 401, 28-42.

Zhang, Z.C., Mahoney, J.J., Mao, J.W., Wang, F.S. (2006a) Geochemistry of picritic and associated basalt flows of the western Emeishan flood basalt province, China. Journal of Petrology, 47, 1997–2019.

Zhang, Z.C., Mao, J.W., Wang, F.S., Pirajno, F.(2006b) Native gold and native copper grains enclosed by olivine phenocrysts in a picritic lava of the Emeishan large igneous province, SW China. American Mineralogist, 91, 1178-1183.

Zhang, Z.C., Mao, J.W., Saunders, A.D., Ai, Y., Li, Y., and Zhao, L. (2009) Petrogenetic modeling of three mafic–ultramafic layered intrusions in the Emeishan large igneous province, SW China, based on isotopic and bulk chemical constraints. Lithos, 113, 369–392.

Zhong, H., and Zhu, W.G. (2006) Geochronology of layered mafic intrusions from the Pan-Xi area in the Emeishan large igneous province, SW China. Mineralium Deposita, 41, 599–606.

Zhong, H., Qi, L., Hu, R.-Z., Zhou, M.-F., Gou, T.-Z., Zhu, W.-G., Liu, B.-G., and Chu, Z.-Y., (2011) Rhenium–osmium isotope and platinum-group elements in the Xinjie layered intrusion, SW China: implications for source mantle composition, mantle evolution, PGE fractionation and mineralization. Geochimica et Cosmochimica Acta, 75, 1621–1641.

Zhou, M.-F., Malpas, J., Song, X.Y., Robinson, P.T., Sun, M., Kennedy, A.K., Lesher, C.M., and Keays, R.R. (2002) A temporal link between the Emeishan large igneous province (SW China) and the end-Guadalupian mass extinction. Earth and Planetary Science Letters, 196, 113–122.

Zhou, M.-F., Robinson, P.T., Lesher, C.M., Keays, R.R., Zhang, C.J., and Malpas, J. (2005) Geochemistry, petrogenesis, and metallogenesis of the Panzhihua gabbroic layered intrusion and associated Fe-Ti-V-oxide deposits, Sichuan Province, SW China. Journal of Petrology, 46, 2253–2280.

Zhou, M. -F., Arndt, N.T., Malpas, J., Wang, C.Y., and Kennedy, A.K. (2008) Two magma series and associated ore deposit types in the Permian Emeishan large igneous province, SW China. Lithos, 103, 352–368.

Figure Captions

Figure 1. Distribution of Emeishan flood basalts and coeval mafic intrusions modified from Chung and Jahn (1995) and Song et al. (2001).

Figure 2. Photomicrograph of rock samples of the picrites and basalts observed under crossed polars. (a) clinopyroxene phenocryst in picrite (Sample XL5); (b) olivine phonocryst in picrite (Sample DY8-8); (c) and (d) clinopyroxene phonocrysts in basalts (Sample GYH1, DYC9). Mineral abbreviations: Ol = olivine, Cpx = clinopyroxene.

Figure 3. Rhodes Diagrams for olivines in picrites (a) and clinopyroxene in basalts and picrites (b) from the Emeishan LIP. Abbreviations: Oliv=olivine; Cpx=clinopyroxene; HT=High Ti; LT=Low Ti.

Figure 4. Crystallization temperatures of olivine phenocrysts in picrites calculated using the olivine-liquid thermometer of Putirka (2008). Abbreviations: Oliv=olivine; HT=High Ti; LT=Low Ti.

Figure 5. Temperatures and depths of crystallization of clinopyroxene phenocrysts in the ELIP picrites and basalts, calculated using the clinopyroxene-liquid thermobarometer of

Putirka et al. (2008). Pressure to depth conversion is assumed to be 2.8 km/kbar. Depth of the lower and middle and upper crust are adapted from Jiang et al. (2012). Abbreviations: Abbreviations: Cpx=clinopyroxene; HT=High Ti; LT=Low Ti.

Figure 6. Change of estimated magma density vs. depth (a). The lithosphere profile (b) is from Jiang et al. (2012) and refer to Gao et al.(1998) and Wu et al.(2012). Magma density was calculated from the models of Lange and Carmichael (1990), using liquid compositions equilibrated with Cpx and P-T conditions from clinopyroxene-melt thermobarometers. Density of primary magma (in whole rock composition of sample DY8-8, see text) in a given depth in mantle are calculated by assuming temperature is 1500°C in the Moho at depth of 55 Km according to olivine-liquid thermometer calculation (see text)..

Figure 7. A schematic model of the magma plumbing system of the ELIP. See text for explanation.

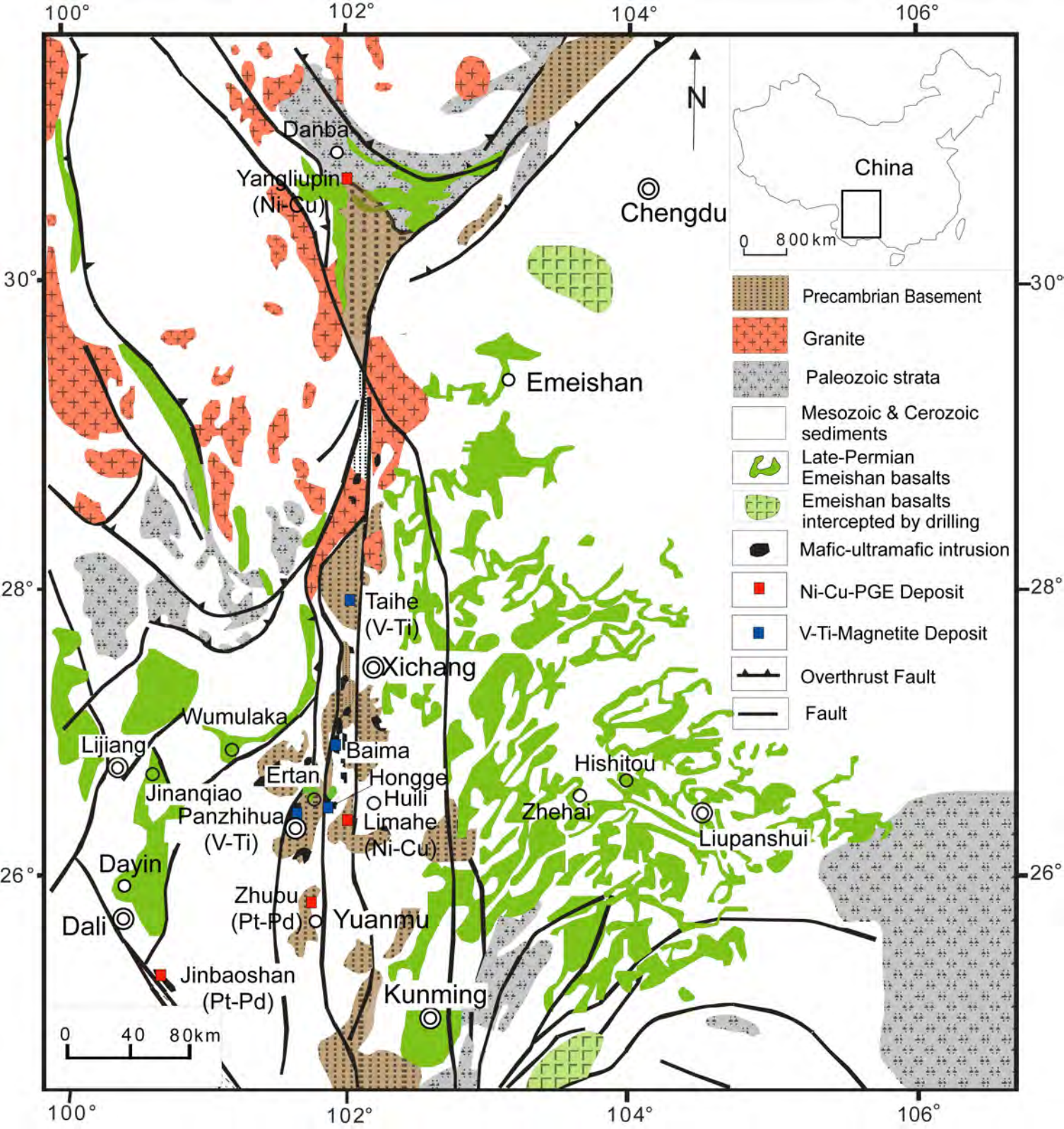
100°
102°
104°
106°
30°
28°
26°
N
China
0 800km
Danba
Yangliupin
(Ni-Cu)
Chengdu
Emeishan
Taihe
(V-Ti)
Xichang
Wumulaka
Lijiang
Baima
Ertan
Hongge
Huili
Limahe
(Ni-Cu)
Jinanqiao
Panzhihua
(V-Ti)
Hishitou
Zhehai
Liupanshui
Dayin
Dali
Zhubu
(Pt-Pd)
Yuanmu
Jinbaoshan
(Pt-Pd)
Kunming
0 40 80km
Precambrian Basement
Granite
Paleozoic strata
Mesozoic & Cerozoic sediments
Late-Permian Emeishan basalts
Emeishan basalts intercepted by drilling
Mafic-ultramafic intrusion
Ni-Cu-PGE Deposit
V-Ti-Magnetite Deposit
Overthrust Fault
Fault

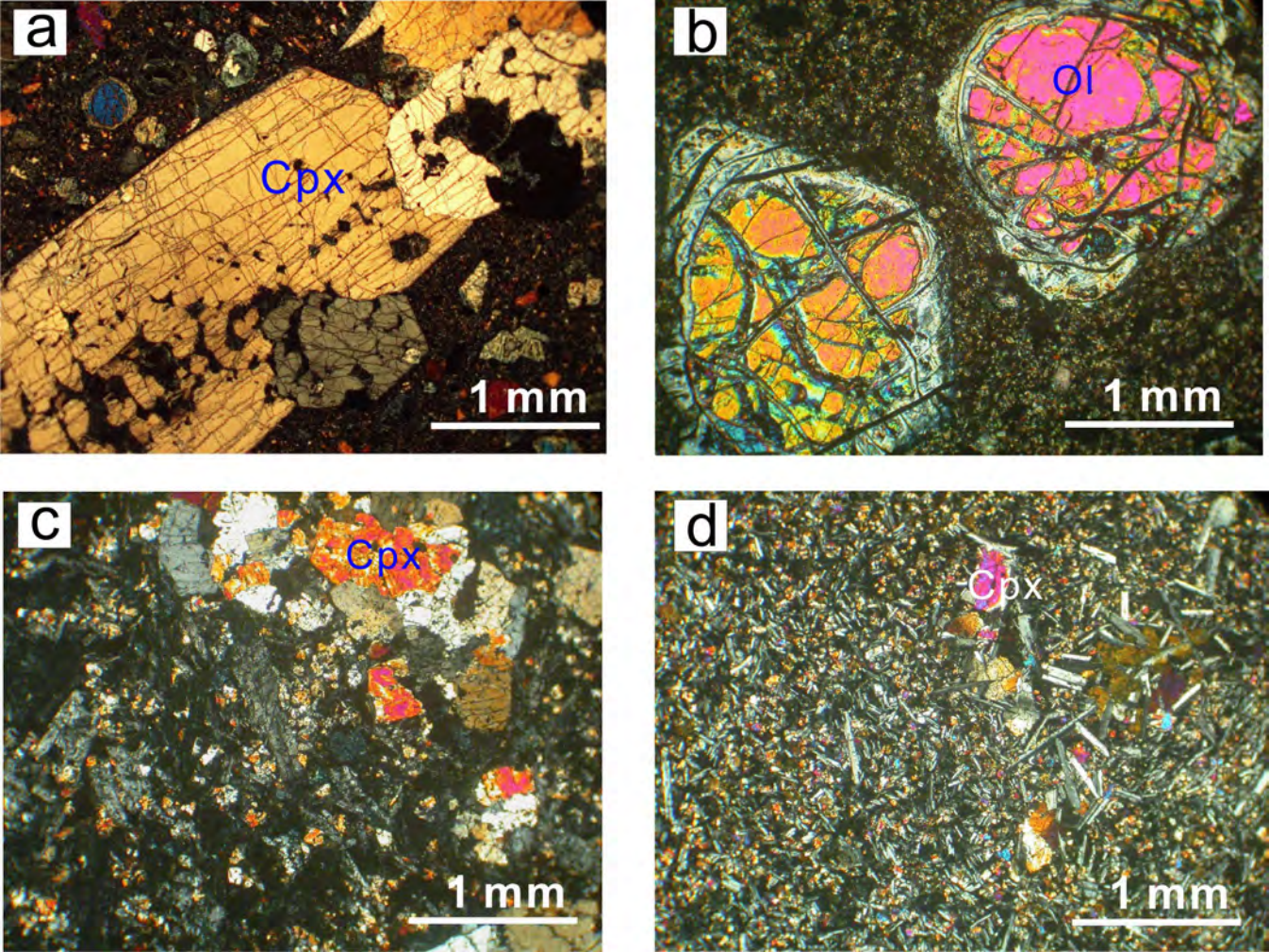
a
Cpx
1 mm
b
Ol
1 mm
c
Cpx
1 mm
d
Cpx
1 mm

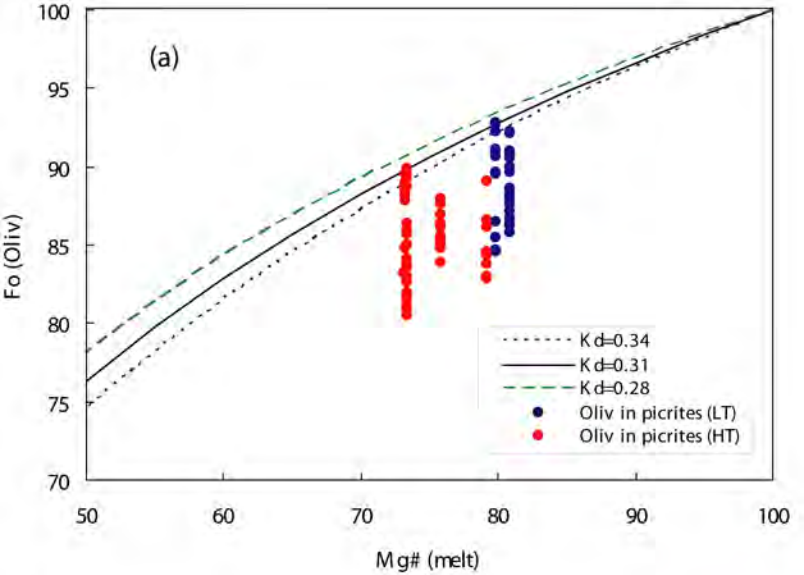
(a)
Fo (Oliv)
Mg# (melt)
Kd=0.34
Kd=0.31
Kd=0.28
Oliv in picrites (LT)
Oliv in picrites (HT)

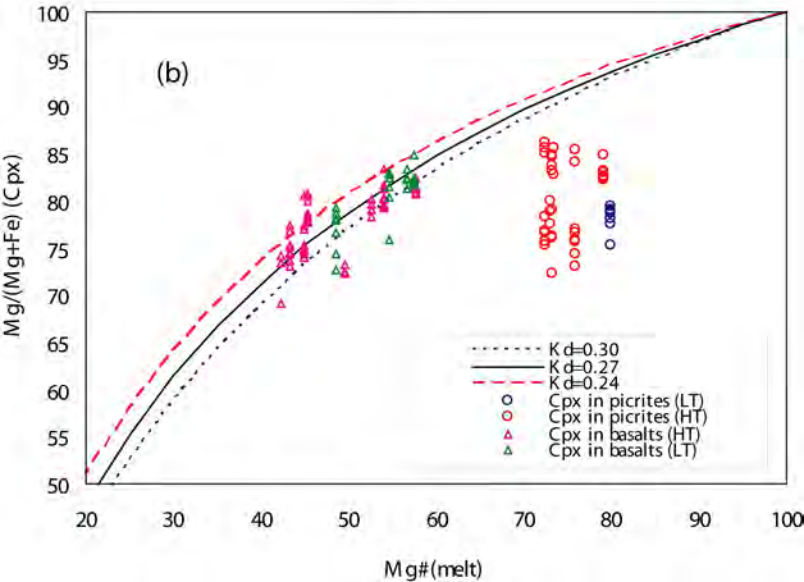
(b)
Mg/(Mg+Fe) (Cpx)
Mg#(melt)
Kd=0.30
Kd=0.27
Kd=0.24
Cpx in picrites (LT)
Cpx in picrites (HT)
Cpx in basalts (HT)
Cpx in basalts (LT)

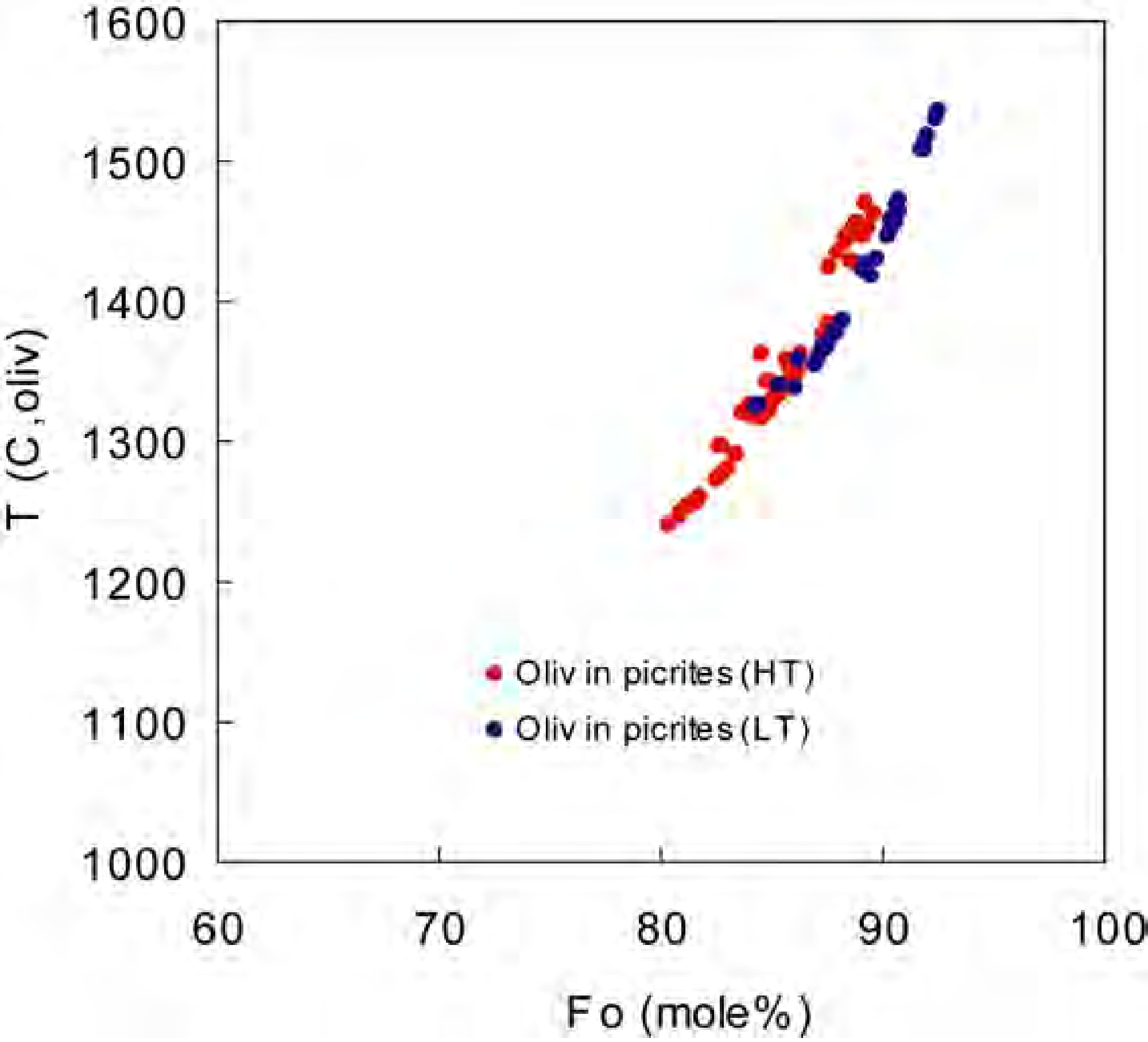
1600
1500
1400
1300
1200
1100
1000
T (C, oliv)
60
70
80
90
100
Fo (mole%)
Oliv in picrites (HT)
Oliv in picrites (LT)

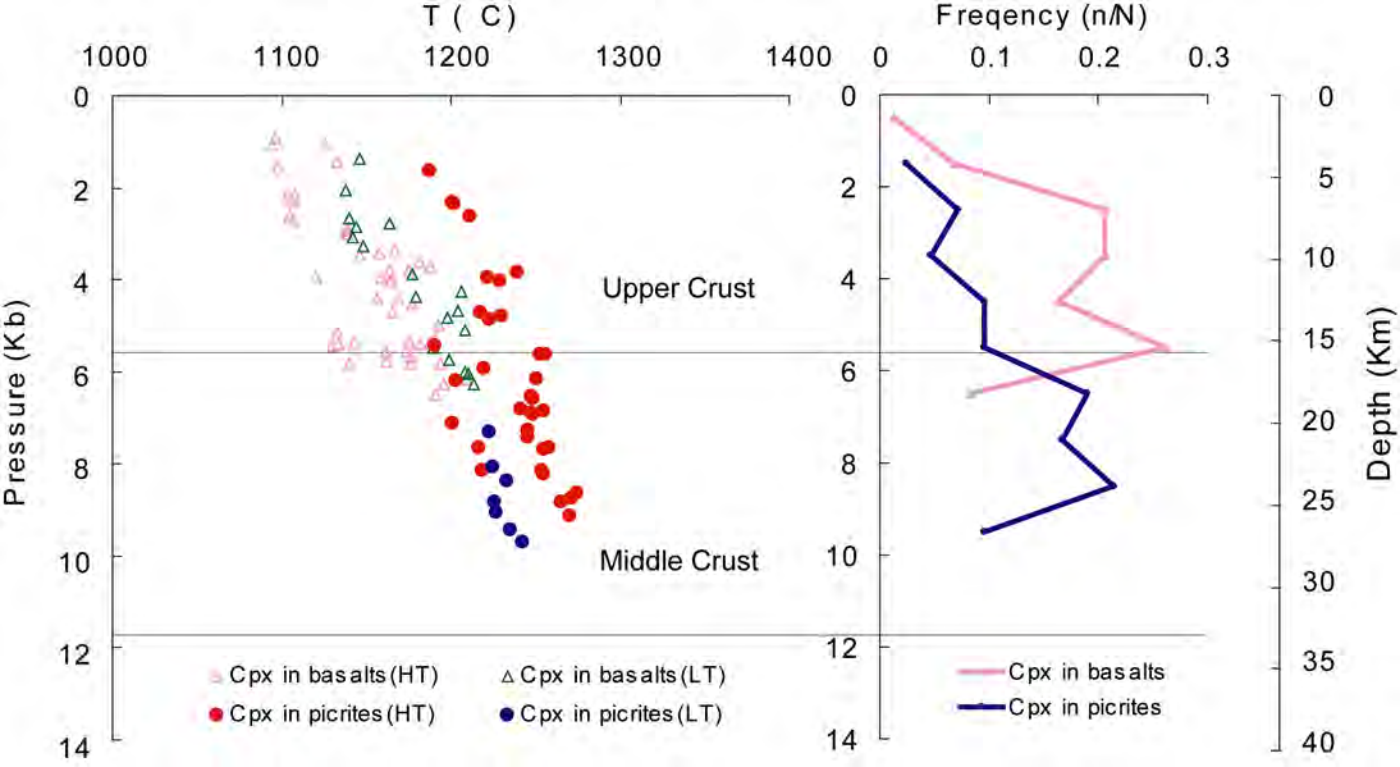
T (C)
1000
1100
1200
1300
1400
Freqency (n/N)
0
0.1
0.2
0.3
Pressure (Kb)
Depth (Km)
Upper Crust
Middle Crust
Cpx in basalts (HT)
Cpx in basalts (LT)
Cpx in picrites (HT)
Cpx in picrites (LT)
Cpx in basalts
Cpx in picrites

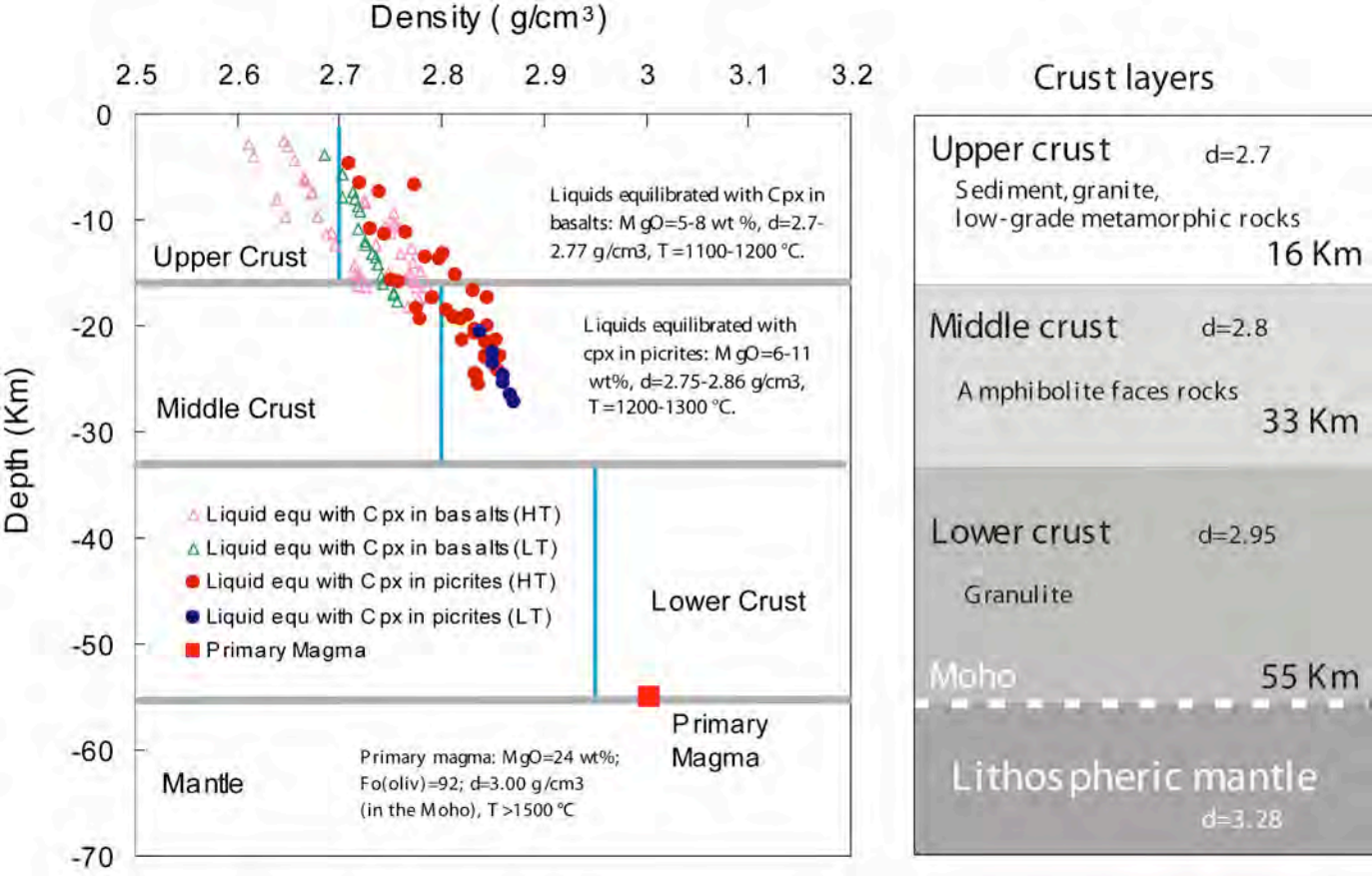
Density (g/cm3)
2.5
2.6
2.7
2.8
2.9
3
3.1
3.2
0
-10
-20
-30
-40
-50
-60
-70
Depth (Km)
Upper Crust
Middle Crust
Lower Crust
Mantle
Liquids equilibrated with Cpx in basalts: MgO=5-8 wt %, d=2.7-2.77 g/cm3, T=1100-1200 °C.
Liquids equilibrated with cpx in picrites: MgO=6-11 wt%, d=2.75-2.86 g/cm3, T=1200-1300 °C.
Liquid equ with Cpx in basalts (HT)
Liquid equ with Cpx in basalts (LT)
Liquid equ with Cpx in picrites (HT)
Liquid equ with Cpx in picrites (LT)
Primary Magma
Primary Magma
Primary magma: MgO=24 wt%; Fo(oliv)=92; d=3.00 g/cm3 (in the Moho), T >1500 °C
Crust layers
Upper crust
d=2.7
Sediment, granite, low-grade metamorphic rocks
16 Km
Middle crust
d=2.8
Amphibolite faces rocks
33 Km
Lower crust
d=2.95
Granulite
Moho
55 Km
Lithospheric mantle
d=3.28

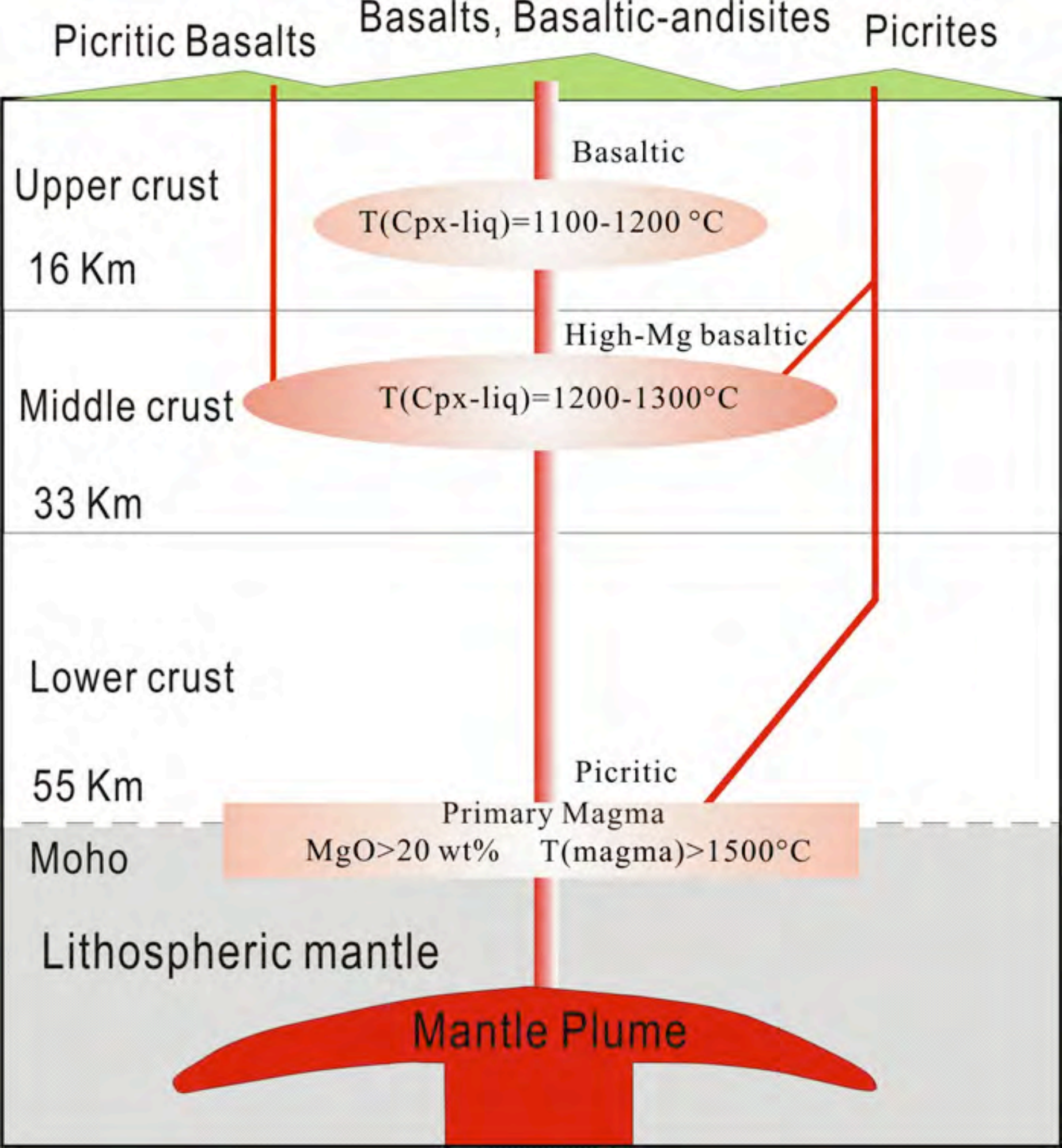
Picritic Basalts
Basalts, Basaltic-andisites
Picrites
Basaltic
Upper crust
T(Cpx-liq)=1100-1200 °C
16 Km
High-Mg basaltic
Middle crust
T(Cpx-liq)=1200-1300°C
33 Km
Lower crust
55 Km
Picritic
Primary Magma
MgO>20 wt%
T(magma)>1500°C
Moho
Lithospheric mantle
Mantle Plume